Journal of Thermal Analysis and Calorimetry, Vol. 84 (2006) 1, 247–252

TYPICAL DATA OF A NEW MICROPOROUS MATERIAL OBTAINED FROM GELS WITH TITANIUM AND SILICON

M. Veltri[1], *D. Vuono*[1], *P. De Luca*[1*], *J. B. Nagy*[2] *and A. Nastro*[1]

[1]Dipartimento di Pianificazione territoriale, Università della Calabria, 87036 Arcavacata di Rende CS, Italy
[2]Laboratoire de RMN, Facultés Universitaires N.D. de la Paix, 5000 Namur, Belgium

The aim of this work is the synthesis and the characterization of a microporous material obtained from gels with titanium and silicon: NTS (titanosilicate). The structure of NTS zeotype is similar to that of AM-1 and JDF-L1 (titanosilicates).

The synthesis were carried out with gels of composition: $3.5Na_2O$–$yTiO_2$–4.48HCl–$xSiO_2$–$110H_2O$ with $1.0 \le x \le 12.0$ and $0.2 \le y \le 0.7$. The temperature of reaction was 190±2°C.

In most of the cases NTS was prepared in a pelletted form. NTS pellets are produced at TiO_2 content higher than 0.3 moles and SiO_2 comprised between 3 and 7. NTS in a powder form is produced for TiO_2<0.3 and SiO_2 between 3 and 5 moles. It describes crystallization field and the kinetic curves of the titanosilicate.

The samples are characterized by X-ray diffraction (XRD), thermogravimetry (TG), derivative thermogravimetry (DTG), differential scanning calorimetry (DSC), nuclear magnetic resonance spectroscopy-high resolution solid state MAS ^{29}Si-NMR, scanning electron microscope (SEM), energy dispersive spectroscopy (EDS) X-ray microanalysis.

Keywords: *microporous material, solid-state NMR, thermal analysis, titanosilicate*

Introduction

The first mentioning of titanium containing molecular sieves dates back to 1967 when Young has patented this material [1]. The Ti atoms incorporated in the structure have tetrahedral coordination [TiO_4] in micro and mesoporous materials such as TS-1, TS-2 [2–4], Ti-Beta [5] (titanosilicates) that have very good catalytic properties. In addition, the Ti atoms may also have octahedral coordination [TiO_6^{2-}] in the structure. Others titanosilicates have analogs in natural crystals, ETS-4≡zorite [6], ETS-14≡penkvillesite [7, 8] (Engelhard Titanosilicate), AM-2, STS and UND-1≡umbite [7, 9, 10] and others present new structures, ETS-10 [11] and AM-4 [7].

Kozankova *et al*. prepared a porous filter composed of two porous layers: macro-porous carrier and microporous sodium borosilicate (NBS) glass with TiO_2 additive (NBST glass) [12]. Varshney *et al*. have synthesized as new phases of hybrid fibrous ion exchangers [13]. Mojumdar *et al*. have synthesized as new phases of hybrid fibrous ion exchangers, pectin based cerium(IV) and thorium(IV) phosphates [14].

Among the crystalline microporous titanosilicates having octahedral Ti and tetrahedral Si, the ETS-4 and ETS-10 structures discovered by Kuznicki in 1989 are the most important ones [11, 15].

ETS-10 is a microporous framework zeolite-type titanosilicate, possessing a three-dimensional 12-ring pore system (large pore opening of 1.0 nm). The formation of the pores is frequently disorganized [16, 17]. The fusion of adjacent pores can lead to a large pore of 1.43 nm. Their potential uses include catalysis, desiccation and ion-exchange [11, 16, 17].

ETS-4, a small pore member of the ETS family (pore dimension of 0.37 nm) is characterized by a distinct interconnected octahedral (TiO_6)-tetrahedral (SiO_4) framework structure [6, 18]. Due to the tunable diameter, ETS-4 crystals can be commercially used for separation of gas mixtures with similar molecular size [18, 19]. The crystals are formed probably of intergrowth of zorite and nenadkevichite [6].

The synthesis of AM-1 was carried out in 1995 [17], the structure of which is identical to JDF-L1 [20]. AM-1 (as well as AM-2 and AM-3) does not contain Ti–O–Ti bonds. It is a non-centrosymmetrical tetragonal layered solid ($Na_4Ti_2Si_8O_{22}\cdot 4H_2O$), which contains five-coordinated Ti(IV) ions in the form of TiO_5 square pyramids in which each of the vertices of the base is linked to SiO_4 tetrahedra [$TiO\cdot O_4(SiO_3)_4$] to form continuous sheets [7, 17, 20]. The interlamellar Na^+ ions are exchangeable [7, 20]. The ^{29}Si-NMR spectrum consists of one single line at –107.4 ppm corresponding to Si(3Si, 1Ti) configuration.

The new NTS titanosilicate [21, 22] corresponds to the structure of AM-1 and JDF-L1 [23]. In this work, we describe its crystallization field and the kinetic curves.

* Author for correspondence: p.deluca@unical.it

1388–6150/$20.00

Akadémiai Kiadó, Budapest, Hungary
Springer, Dordrecht, The Netherlands

The intermediate and final crystalline products are characterized by XRD, thermal analysis (TG, DTG, DSC), SEM, chemical analysis by EDS and high resolution MAS ^{29}Si-NMR.

Experimental

The syntheses were carried out following the previously described procedure [24]. Gels of following compositions were prepared: $3.5Na_2O$–$yTiO_2$–$4.48HCl$–$xSiO_2$–$110H_2O$ with $1.0 \le x \le 12.0$ and $0.2 \le y \le 0.7$.

The acidic solution (A) was prepared by dissolving HCl (Carlo Erba, 37 mass%), $TiCl_4$ (Carlo Erba, 50 mass%) in distilled water. The basic solution (B) is composed of a solution of sodium silicate (Merck, 8 mass% Na_2O, 27 mass% SiO_2, 65 mass% H_2O) and NaOH (Carlo Erba, 50 mass%). Solution A is poured into solution B and the resulting gel is homogenized by stirring. The pH is close to 13. The so-produced gel is introduced to teflon lined stainless steel Morey type autoclaves. The synthesis is carried out at 190±2°C in hydrothermal conditions, in static conditions, during various times. At the end of the reaction, the autoclaves are quenched in tap water. The pH and the ionic conductivity of the aqueous phase are measured. The recovered products (either in a pellet or a powder form) are filtered and washed with cold distilled water until neutrality is reached. Finally, they are dried at 100°C for 24 h. The mother liquors are also analysed for their composition.

For the XRD measurements part of the pelletted NTS samples were reduced to powder.

The powder diffraction patterns were recorded on a Philips PW 1830 diffractometer using CuK_α radiation. The scanning rate was 0.02° s^{-1} in the range of 5–45° 2θ.

The thermal analysis was carried out on a Netzsch 429 instrument in static air. The heating rate was of 10°C min^{-1}.

The ^{29}Si-NMR spectra were obtained on a Bruker MSL 400 spectrometer at 79.49 MHz, t_p=4.0 μs (θ=π/4) and repetition time of 6.0 s. Some 10.000 FIDs were accumulated before Fourier transform.

Results and discussion

Figure 1 shows the crystallization fields. It can be noted that in most of the cases NTS was prepared in a pelletted form.

NTS in a pelletted form is produced at TiO_2 content higher than 0.3 moles and SiO_2 comprised between 3 and 7. At higher SiO_2 content quartz also cocrystallizes. NTS in a powder form is produced in a narrower fields,

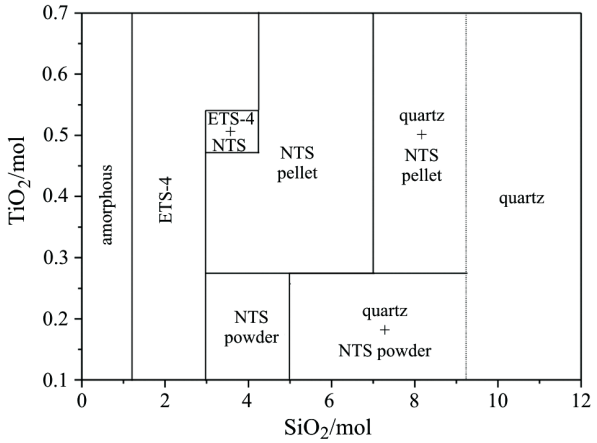

Fig. 1 Crystallization fields as a function of TiO_2 and SiO_2 obtained from gels of compositions $3.5Na_2O$–$yTiO_2$–$4.48HCl$–$xSiO_2$–$110H_2O$ at 190°C after 72 h

for TiO_2<0.3 and SiO_2 between 3 and 5 moles. At higher SiO_2 content, quartz is also formed. At very low SiO_2 content, no crystalline form could be obtained. For SiO_2 content between ca. 1 and 3 moles pure ETS-4 phase is produced. At very high SiO_2 content (higher than 9 moles) only quartz could be recovered.

The initial pH (pH_i) has a great influence on the final phase produced. If pH_i>13, only amorphous phase is recovered. For 11.5<pH<12.5, pure ETS-4 is formed. The NTS pellets and powder are synthesized for 11.0≤pH≤12.0. Finally, at low pH values only quartz is produced.

The crystallization curves were computed from the five most intense peaks in the X-ray diffractograms (Fig. 2). The induction time determined as the appearance of ca. 4% crystallinity and the crystallization rate R in % h^{-1} are reported in Table 1.

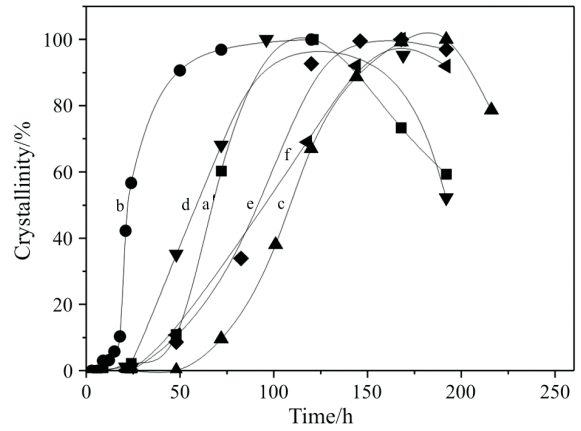

Fig. 2 Crystallization curves obtained from gels of compositions $3.5Na_2O$–$yTiO_2$–$4.48HCl$–$xSiO_2$–$110H_2O$; a – GM03 (x=4, y=0.2), b – GM07 (x=4, y=0.4), c – GM17 (x=6, y=0.4), d – GM21 (x=5, y=0.6), e – GM22 (x=5, y=0.4) and f – GM23 (x=5, y=0.2)

Table 1 Kinetic parameters for selected NTS samples obtained from gels of composition $3.5Na_2O$–$yTiO_2$–4.48HCl–$xSiO_2$–$110H_2O$

Sample		x	y	t_{ind}/h	R/% h^{-1}	$Z(t)=k_1t^n$			$\ln[1/(1-Z(t))]=(k_2t)^m$		
						k_1	n	r^2	k_2	m	r^2
GM03	powder	4	0.2	38.6	2.33	$1.7\cdot10^{-4}$	2.9	0.97	$1.2\cdot10^{-2}$	3.3	0.95
GM23	powder	5	0.2	35.6	0.99	$4.0\cdot10^{-3}$	2.0	0.98	$9.0\cdot10^{-3}$	2.6	0.96
GM07	pellet	4	0.4	13.0	8.25	$2.2\cdot10^{-3}$	2.9	1.00	$2.6\cdot10^{-2}$	3.0	1.00
GM17	pellet	6	0.4	55.6	1.04	$6.9\cdot10^{-7}$	3.8	1.00	$8.5\cdot10^{-3}$	4.7	1.00
GM21	pellet	5	0.6	24.5	1.48	$3.0\cdot10^{-7}$	4.8	0.96	$1.9\cdot10^{-2}$	5.2	0.96
GM22	pellet	5	0.4	29.7	1.17	$1.7\cdot10^{-6}$	4.0	1.00	$1.2\cdot10^{-2}$	4.6	0.99

It is difficult to compare the kinetic data for the powder and for the pellets, because the two forms are obtained with different initial TiO_2 and SiO_2 contents.

As far as the formation of pellets is concerned increasing the amount of SiO_2 has a detrimental effect on both induction and crystallization rates. Indeed, the induction time increases, while the crystallization rate decreases for y=0.4 and x varying from 4 to 6. The influence of the amount of TiO_2 is opposite, the induction time decreases for x=5 and y=0.4 and 0.6, while the crystallization rate increases. Finally, the influence of the amount of SiO_2 on the rate of formation of NTS in the powder form is also detrimental.

The kinetic data are analysed following the equation $Z(t)=k_1t^n$ where $Z(t)$ is the crystallinity at time t and k_1 and n are constants depending on the nucleation and rate of crystal growth. This equation represents rather well the kinetic data in the initial range (for $\ln Z=\ln k_1+n\ln t$, $r^2\cong1$). The values of k_1 and n parameters are reported in Table 1. The n values higher than 4 are characteristic of an increase in crystal growth rate as a function of time. For the two powder samples (GM03 and GM23 – GM is the name of sample) the decrease of the crystallization rates with increasing SiO_2 content is expressed by an increase in k_1 values from $1.7\cdot10^{-4}$ to $4.0\cdot10^{-3}$ and a decrease of the n value from 2.9 to 2.0. An opposite behaviour is observed for the pelleted forms (GM07 and GM17) where the decrease of the crystallization rates is expressed by a great decrease in the k_1 values from $2.2\cdot10^{-3}$ to $6.9\cdot10^{-7}$ while the n value increase from 2.9 to 3.8. Finally, for the pellets GM21 and GM22, the slight decrease in the crystallization rate due to the decrease of TiO_2 content is expressed in the increase of k_1 values from $3.0\cdot10^{-7}$ to $1.7\cdot10^{-6}$, while the n values decreases from 4.8 to 4.0. The same kinetic data are analysed using the Avrami–Erofeev equation [25] $\ln[(1/(1-Z(t))]=(k_2t)^m$, $Z(t)$ having the same meaning as in equation supra, k_2 and m are kinetic parameters. The reasonable good linear equations (for $\ln[\ln(1/(1-Z))]=m(\ln k_2+\ln t)$, $r^2\cong1$) allowed us to compute the k_2 and m parameters which are also reported in Table 1. In most of the cases, the Avrami–Erofeev equation describes better the change in crystallization rates. Indeed, for example for the powder samples GM03 and GM23 both k_2 and m values are decreasing following the drecrease of the crystallization rate (Table 1). This is also the case for the crystallization of two pellets GM21 and GM22. Only the results of pellets GM07 and GM17 are exceptions. The k_2 values follow the decrease in crystallization rate, they decrease from $2.6\cdot10^{-2}$ to $8.5\cdot10^{-3}$, while the m values are increasing from 3.0 to 4.7.

The pH values and the electric conductivities of the mother liquor vary during the synthesis. The pH values suddenly decrease at the beginning of the synthesis for both the powder and the pellets (from 13 to 11). This is due essentially to the dissolution of the gel using OH^- ions from the liquid phase [26, 27]. At the end the pH is reaching a constant value corresponding to the equilibrium between the dissolution of the gel phase (using OH^- ions) and the crystal formation (liberating OH^- ions). The electric conductivity follows quite closely the pH variation for the pellet formation, it decreases suddenly at the beginning of the crystallization (from 140 to 124 mS cm^{-1}). On the other hand, the decrease is more monotonous for NTS powder formation (from 145 to 120 mS cm^{-1}).

The TG, DTG, and DSC curves are reported in Fig. 3 for a powder NTS sample for various crystallization times. Table 2 gives the temperature of the maxima of the DTG and DSC peaks and the amount of water loss for powder and pellet NTS samples.

The powder NTS sample shows essentially two DSC peaks, the first one at ca. 150°C corresponding to zeolitic water, i.e. water adsorbed in the channels, while the second one at ca. 250°C corresponds to structural water.

The NTS pellets behave differently. In addition to these two characteristic peaks, they always present a third peak at low temperature (around 100°C) corresponding to water hydrating the amorphous phase of the pellets. Indeed, this peak is always present in both powder and pellet samples in the early stage of crystallization.

Table 2 DTG and DSC peak maxima and mass losses for the systems of initial composition $3.5Na_2O$–$yTiO_2$–4.48HCl–$xSiO_2$–$110H_2O$ for reaction times corresponding to ca. 4, 50, 100% crystallinity

Sample		x	y	Reaction time/h	Crystallinity/%	DTG peaks/°C			DSC peaks/°C			Mass loss/%	
						k_1	n	r^2	k_2	m	r^2	T≤200°C	T>200°C
GM03	powder	4	0.2	24	4	120		355	127		368	6.49	8.26
				72	50	148		244	154		250	2.24	5.81
				120	100	144		244	150		251	1.57	5.45
GM07	pellet	4	0.4	9	4	132		349	137		348	8.49	5.60
				21	50	90		254	97		260	15.30	6.72
				120	100	140		229	148		236	3.13	6.60
GM22	pellet	5	0.4	24	4	143		303	151		296	4.56	3.44
				75	50	96	165	250	99	178	256	10.44	7.19
				168	100	79	152	228	85	161	236	3.60	5.66

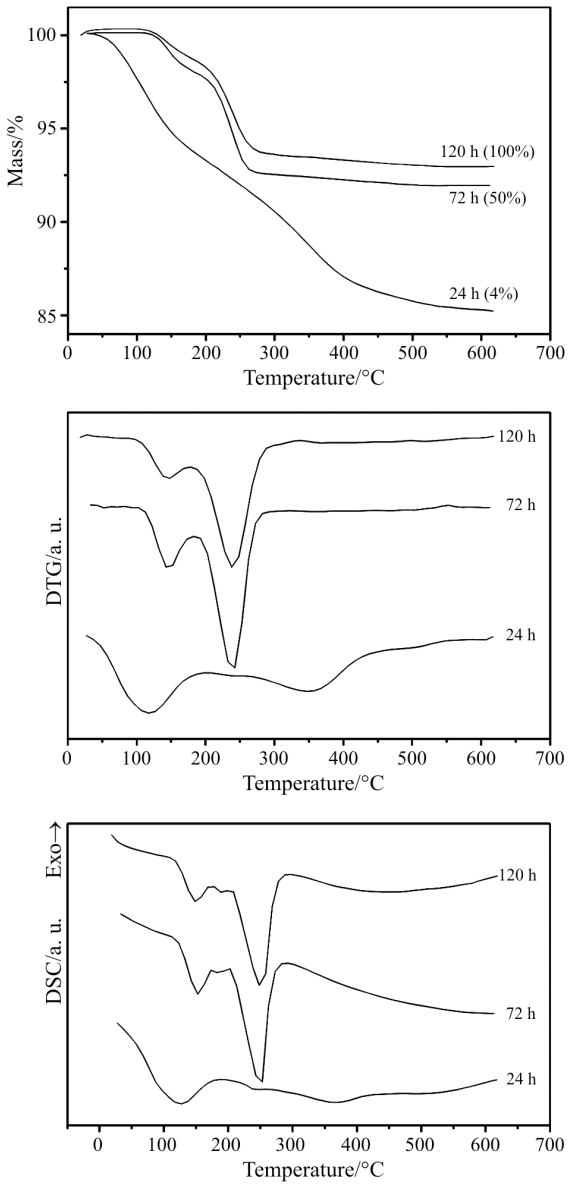

Fig. 3 TG, DTG and DSC curves for the powder sample GM03 of initial composition $3.5Na_2O$–$0.2TiO_2$–4.48HCl–$4.0SiO_2$–$110H_2O$ for reaction times corresponding to ca. 4, 50, 100% crystallinity

Interestingly, both the amount of zeolitic water and that of the structural water are bigger in the NTS pellets than in the powder form (Table 2). The mass losses – zeolitic water (T<200°C) and structural water (T>200°C) – are decreasing monotonously with increasing reaction time for the powder sample (Table 2). On the other hand the mass losses due to the water hydrating the pellet together with the zeolitic water, and the structural water are passing through a maximum for 50% crystallinity.

The thermal stability of the various samples was also tested. For that purpose they were calcined during 2 h at a certain temperature which was varied by 100°C for each step, starting from 200 up to 700°C. The X-ray diffractograms are shown in Fig. 4 for both the pelletted and powdered NTS. It is clearly seen that the initial NTS structure is transformed at 700°C into the narsarsukite structure for the powder form, and at 800°C for pellets (Figs 4a and b) [28].

The thermal analyses (TG, DTG and DSC) are also reported for the pellets (Fig. 5) of the as-synthesized samples and of those calcined at 400 and 600°C. It is clear from these curves that the first peak related to the loss of zeolitic water is completely suppressed (Fig. 5) and the loss of water decreases with increasing calcination temperature of the samples (Table 3). It can also be noticed that NTS in the pelletted form and calcined at 600°C still can adsorb ca. 5% water, while the powder form being much less stable, only readsorbs ca. 1.8% water.

Table 3 Total mass loss as a function of calcination temperature. Initial gel composition: $3.5Na_2O$–$xTiO_2$–4.48HCl–$4.0SiO_2$–$110H_2O$

Sample		x	Calcination temperature/°C	Total mass loss/%
GM07	pellet	0.4	25	9.52
			400	4.77
			600	1.77
GM03	powder	0.2	25	8.79
			400	4.18
			600	1.37

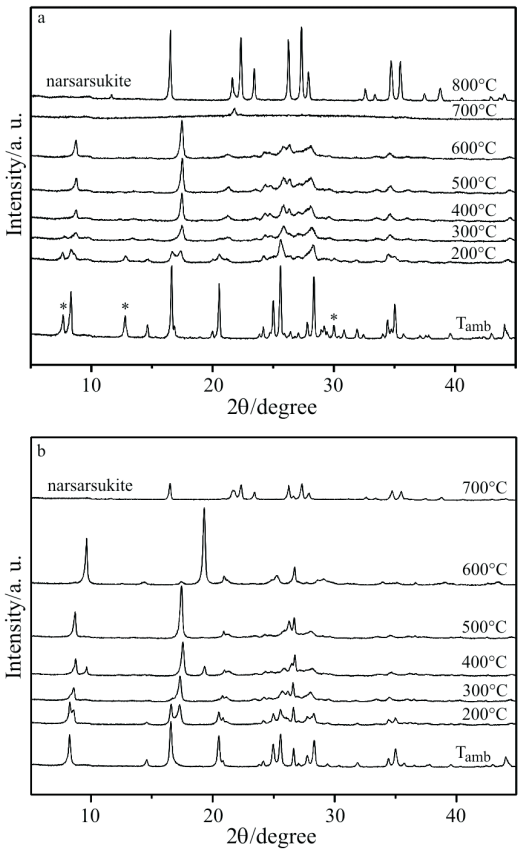

Fig. 4 XRD of the NTS and ETS-4 (impurity) phases for the a – pellet and b – powder forms calcined at various temperatures. * – ETS-4 phase, a –pellet GM07 gel composition $3.5Na_2O–0.4TiO_2–4.48HCl–4.0SiO_2–110H_2O$; b – powder GM03 gel composition $3.5Na_2O–0.2TiO_2–4.48HCl–4.0SiO_2–110H_2O$

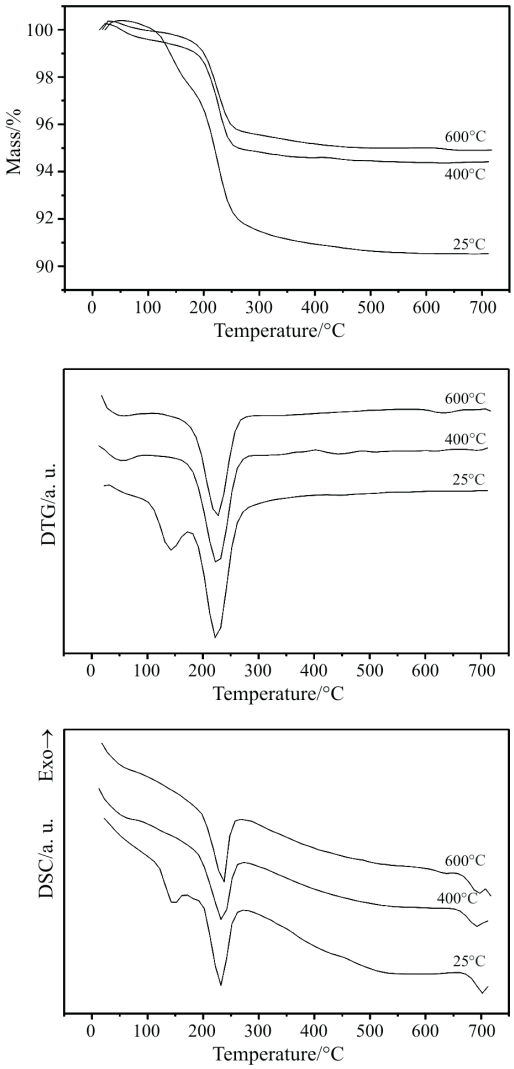

Fig. 5 TG, DTG and DSC curves related to NTS pellet as-synthesized and calcined at 400 and 600°C. Pellet GM07 gel composition: $3.5Na_2O–0.4TiO_2–4.48HCl–4.0SiO_2–110H_2O$

Table 4 shows the chemical analysis by both atomic absorption (Na and Ti contents) and EDS (Si/Ti ratios). For the powder NTS sample, the Ti/Na ratio increases, while the Si/Ti ratio decreases as a function of time. Similar increasing trend is shown for the pellets for both the Ti/Na and Si/Ti ratios.

The SEM photographs are shown for pellets and the powder NTS in Fig. 6. One can easily recognize the lamellar form of the NTS material forming rose-like agglomerates on both the internal part and the external surface of the pellets as well as in the powder NTS. The average size in all cases is ca. 50 μm.

The variation of the ^{29}Si-NMR spectra during the NTS pellet formation is shown in Fig. 7. It can be seen that the initial amorphous gel is progressively transformed into NTS, the chemical shift of which is equal to –107.5 ppm, represented by a single NMR line [7, 17, 20].

This result also shows the similarity between AM-1 and NTS materials. Let us emphasize that

Table 4 Variation of the composition of the NTS phase as a function of time corresponding to 4, 50, 100% crystallinity

Sample		Reaction time/ h	Crystallinity/ %	Na/ mass%	Ti/ mass%	Ti/Na A.A./ mol/mol	Si/Ti EDS/ mol/mol	
GM03	powder	24	4	6.71	5.25	0.36	8.03	
		72	50	8.38	10.83	0.63	3.02	
		120	100	8.52	9.98	0.58	3.00	
GM07	pellet	9	4	10.77	6.55	0.29	ext 5.06	int 5.05
		21	50	9.81	7.29	0.35	ext 4.06	int 3.04
		120	100	11.12	9.68	0.43	ext 3.03	int 2.06

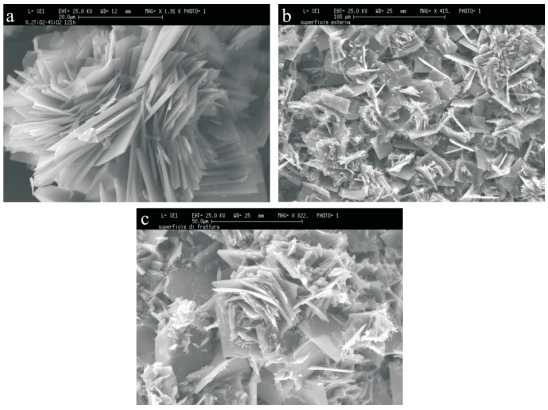

Fig. 6 Scanning electron micrographs of a – powder NTS sample GM03, b – external surface of NTS pellet GM07, c – internal surface of NTS micrographs pellet GM07

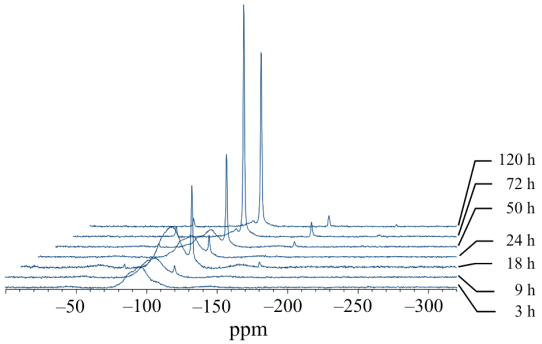

Fig. 7 ^{29}Si-NMR spectra of NTS samples of initial composition $3.5Na_2O–0.4TiO_2–4.48HCl–4.0SiO_2–110H_2O$ during crystallization at 190°C

the ^{29}Si-NMR spectra can also be used to follow the reorganization of the amorphous gel as it was proposed previously [29, 30].

Conclusions

The NTS zeotype, the structure of which is similar to that of AM-1 and JDF-L1, can be easily synthesized from gels of composition $3.5Na_2O–yTiO_2–4.48HCl–xSiO_2–110H_2O$ with $3.0<x<9.0$ and $0.1<y<0.7$. The powder form is obtained with low TiO_2 content ($y<0.3$), while self-bonded pellets are formed for higher TiO_2 content ($y>0.3$). The best conditions with the lowest induction time (13 h) and the highest crystallization rate (R=8.25 % h^{-1}) are found for x=4.0 and y=0.4.

References

1 G. Young, U.S. Pat. 3,329,480 (1967).
2 G. Perego, G. Bellussi, C. Corno, M. Taramasso, F. Buonuomo and A. Esposito, Stud. Surf. Sci. Catal., 28 (1986) 129.
3 M. Taramasso, G. Perego and B. Notari, U.S. Pat. 4,410,501 (1983).
4 J. S. Reddy, R. Kumar and T. Ratnasamy, Appl. Catal., 58 (1990) L1.
5 M. A. Camblor, A. Corma, A. Martinez and J. Perez-Pariente, Chem. Commun., (1992) 589.
6 A. Phillipou and M. Anderson, Zeolites, 16 (1996) 98.
7 Z. Lin, J. Rocha, P. Brandao, A. Ferreira, A. P. Esculcas, J. D. Pedrosa de Jesus, A. Phillipou and M. W. Anderson, J. Phys. Chem. B, 101 (1997) 7114.
8 S. M. Kuznicki, J. S. Curran and X. Yang, PCT W098/32695 (1998).
9 B. Mihailova, V. Valtcheu, S. Mintova and L. Konstantinov, J. Mater. Sci. Lett., 16 (1997) 1303.
10 X. Liu, M. Shang and J. K. Thomas, Microporous Mater., 10 (1997) 273.
11 S. M. Kuznicki, U.S. Pat. 4,853,202 (1989).
12 J. Kozánková, S. C. Mojumdar, J. Chocholoušek, J. Kákoš, M. Balog and L. Krajčová, J. Therm. Anal. Cal., 81 (2005) 191.
13 K. G. Varshney, A. Agrawal and S. C. Mojumdar, J. Therm. Anal. Cal., 81 (2005) 183.
14 S. C. Mojumdar, J. Kozánková, J. Chocholoušek, J. Majling and V. Nemecek, J. Therm. Anal. Cal., 78 (2004) 145.
15 S. M. Kuznicki and A. K. Thrush, Eur. Pat. 0405978A1 (1990).
16 M. W. Anderson, O. Terasaki, T. Ohsuna, A. Philippou, S. P. MacKay, A. Ferriera, J. Rocha and S. Lidin, Nature, 367 (1994) 347.
17 M. W. Anderson, O. Terasaki, T. Ohsuna, P. J. O. Malley, A. Philippou, S. P. MacKay, A. Ferriera, J. Rocha and S. Lidin, Philos. Mag. B, 71 (1995) 813.
18 S. M. Kuznicki, V. A. Bell, S. Nair, H. W. Hillhouse, R. M. Jacubinas, C. M. Braunbarth, B. H. Toby and M. Tsapatis, Nature, 412 (2001) 720.
19 S. M. Kuznicki, V. A. Bell, I. Petrovic and B. T. Desai, U.S. Pat. 6,068,682 (2000).
20 M. A. Roberts, G. Sankar, J. M. Thomas, R. H. Jones, H. Du, J. Chen, W. Pang and R. Xu, Nature, 381 (1996) 401.
21 A. Nastro, P. De Luca, M. Turco, G. Bagnasco and G. Busca, Pat. RM2001A000172 (2001).
22 P. De Luca, G. Veltri, M. Veltri and A. Nastro, Pat. RM2003A000456 (2003).
23 C. C. Pavel, D. Vuono, L. Catanzaro, P. De Luca, N. Bilba, J. B. Nagy and A. Nastro, Microporous Mesoporous Mater., 56 (2002) 227.
24 J. Rocha and M. W. Anderson, Eur. J. Inorg. Chem., (2000) 801.
25 W. J. Kim, M. C. Lee, J. C. Yoo and D. T. Hayhurst, Microporous Mesoporous Mater., 41 (2000) 79.
26 J. L. Casci and B. M. Lowe, Zeolites, 3 (1983) 186.
27 K. R. Franklin and B. M. Lowe, Zeolites, 8 (1988) 495.
28 M. Naderi and M. W. Anderson, Zeolites, 17 (1996) 437.
29 G. Engelhardt and D. Michel, High Resolution Solid-State NMR of Silicates and Zeolites, Wiley and Sons, Chichester 1987.
30 J. B. Nagy, P. Bodart, I. Hannus and I. Kiricsi, Synthesis, Characterization and Use of Microporous Materials, Deca Gew Ltd., Szeged, Hungary 1998.

DOI: 10.1007/s10973-005-7207-5